IEEE Photonics Journal
An IEEE Photonics Society Publication

GeSn Nanobeam Light-Emitting Diode as a GHz-Modulated Light Source

Volume 9, Number 5, October 2017

Ricky Gibson
Joshua Hendrickson
Richard A. Soref, ***Life Fellow, IEEE***

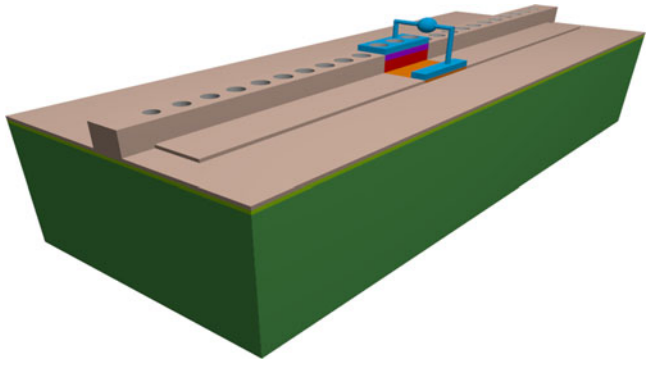

DOI: 10.1109/JPHOT.2017.2749960
1943-0655 © 2017 IEEE

IEEE photonics SOCIETY

IEEE

GeSn Nanobeam Light-Emitting Diode as a GHz-Modulated Light Source

Ricky Gibson,[1,2] **Joshua Hendrickson,**[2]
and Richard A. Soref,[3] ***Life Fellow, IEEE***

[1]University of Dayton Research Institute, Dayton, OH 45469 USA
[2]Air Force Research Laboratory, Sensors Directorate, Wright-Patterson Air Force Base, OH 45433 USA
[3]Department of Engineering, University of Massachusetts Boston, Boston, MA 02125 USA

DOI:10.1109/JPHOT.2017.2749960

Manuscript received August 23, 2017; revised August 30, 2017; accepted September 5, 2017. Date of publication September 5, 2017; date of current version September 20, 2017. This work was supported by the Air Force Office of Scientific Research under award numbers FA9550-15-15RY159COR and FA9550-14-1-0196. Corresponding author: Ricky Gibson (e-mail: rgibson1@udayton.edu).

Abstract: Designs and theoretical analysis are presented for a room temperature resonant-cavity-enhanced GeSn LED whose emission peaks at the 2 μm wavelength. The Ge/GeSn/Ge PIN hetero-diode of length 1 μm is embedded in a rib-type Ge-on-Si nanobeam having either 24 or 36 air holes. The maximum LED modulation bandwidth f_{3dB} is proportional to the Purcell factor and is inversely proportional to τ_{sp0} the GeSn bulk spontaneous emission lifetime. For an emission linewidth of 200 nm and τ_{sp0} of 10 ns, an f_{3dB} of 1.6 GHz is predicted.

Index Terms: Light emitting diodes, electrooptic devices, photonic crystals

1. Introduction

Design considerations and theoretical simulations are presented for a Ge/GeSn/Ge PIN layered light-emitting diode (LED) that is embedded in a Ge-on-Si waveguided network. The LED is resonant-cavity-enhanced by a 1D photonic crystal (PhC) air-hole lattice formed in the waveguide. The room temperature device emits in the 2 μm wavelength band with emission end-coupled into Ge-on-Si. Due to the small active mode volume, the Q/V Purcell factor speeds up the spontaneous emission lifetime, with speeds of $\sim$1 GHz estimated for direct internal modulation of the LED, making it a useful on-chip surrogate for a GeSn laser diode.

2. Background Discussion

Instead of the traditional vertical-cavity LED that emits light into free space, we focus here upon LEDs that are integrated into a rib-channel waveguide in order to radiate the emission into a transparent waveguide (or waveguides) that are end-coupled to the LED channel. Thus we examine the LED as an on-chip light source whose "captured emission" drives an on-chip waveguided network. From the standpoint of semiconductor materials, it is necessary for the connecting waveguides to have a wider bandgap than that of the active LED core. Hence the connecting waveguide material is different, which may require regrowth of that waveguide material after the LED portions have been formed.

The purpose of this paper is to examine resonance-enhanced LED structures that are formed within a nanobeam (NB). The NB is a rib-channel or strip-channel waveguide that contains a 1D PhC lattice of air holes designed to create a horizontal resonant cavity in mid beam [1], [2]. Resonance refers to the narrowband fundamental (Bloch #1 mode) transmission in the PhC forbidden band. Because the active volume of the LED is then very small, the optical power emitted is likewise small. Therefore, the cavity enhancement necessitates a speed-vs-power tradeoff.

Another goal of this paper is to examine LEDs constructed via group IV photonics (GFP), especially devices that emit at room temperature in the 2 μm wavelength band where fiber-optic links are enabled by hollow core photonic bandgap (PBG) fibers. Silicon-based GFP is an emerging and manufacturable technology in which the active and passive on-chip waveguided photonic components are primarily SiGeSn heterostructures. Potential chip applications include sensing and optical interconnects as well as fiber communications. The new 2 μm fiber-optic-comm band is an ideal wavelength range in which to apply room temperature group-IV photonic integrated circuits (PICs) as transceiver chips or as a refractometer-on-chip or spectrometer-on-chip. For opto-electronic computing applications, 2 μm intra-chip and chip-to-chip connects are helpful. In each case, our vision is a monolithic chip containing a complete suite of GFP components.

In these GFP scenarios, an unmet challenge is the realization of an on-chip electrically pumped SiGeSn laser diode (LD), a device under intense study today. The LD designs being considered feature quantum wells and complex epitaxial layering. A technically simpler solution for light sources would be better. Not every application demands laser capabilities, and for those applications, we are examining alternative on-chip sources. The present paper proposes a resonant, waveguided GeSn LED in which the normal rate of internal EO modulation has been increased dramatically over the rate of prior-art, bulk, free-space LEDs. Our theory work indicates that speeds in the GHz range are feasible. Those speeds result from embedding the active emitter in a NB-cavity, giving an ultra-small mode volume and high quality factor, leading to a large Purcell factor that reduces the bulk spontaneous recombination time and increases the speed of direct modulation. With the resonator, the LED's broad emission shrinks down to a $\sim$1.5 nm spectral width. Nevertheless, this on-chip power is expected to give adequate signal-to-noise ratios at the on-chip photodetectors in various applications. Also, multi-spectral or wavelength-multiplexed LED arrays on-chip appear feasible.

3. Prior Art

Several works have formulated models to calculate the modulation bandwidth of a Purcell enhanced nanocavity LED [3]–[5], or nanoLEDs. Reference [3] offers an upper limit of the modulation bandwidth due to Purcell enhancement while References [4] and [5] take into account the density of states of the active medium when evaluating the modulation bandwidth. Each of these works has demonstrated modulation rates in the GHz range for various cavity quality factors and mode volumes with III–V quantum well and quantum dot active media. Due to the fast approximately nanosecond lifetimes in III–V materials, modulation rates due to plasmonic enhancement have been calculated $>$100 GHz [3], [6], [7] while 2D PhC resonators have experimentally demonstrated modulation rates of 10 GHz using III-V quantum dots [8]. Monolayers of 2D materials have also been used to show 100 MHz modulation when coupled to 2D PhCs [9]. These 2D PhCs demonstrations provide free-space emission, but can be coupled to PhC waveguides efficiently [10], however, the fabrication difficulty including the PhC hole array and the suspended slab are significant. The NB PhC cavity is well suited for waveguide coupling due to the 1D PhC holes fabricated in a single mode waveguide and thus a good candidate for waveguide networks.

GaAs suspended NBs with InAs quantum dots as the active medium have demonstrated modulation of 0.1 GHz [11]. This demonstration utilized a fiber taper coupled to the nanobeam for collection of the modulated light and was limited by the electronic's speeds. Several other NB designs have been proposed as nanoLEDs in a III–V platform which have a room-temperature modulation bandwidth upper limit of $\approx$60 GHz. Bulk InGaAsP layered between InP [12] and InAs nanopillar quantum dots embedded in a SiO_2 slot [13] have been proposed as an active medium in a NB LED.

Additionally, a hybrid cavity utilizing a patch antenna at the center of a nanobeam has been reported to theoretically obtain a Purcell enhancement of 428 due to the reduction in mode volume, $\approx 54\times$, of the NB PhC cavity despite the drop in Q, $\approx 100\times$ [14].

To the best of our knowledge there has yet to be an efficiently waveguide coupled nanoLED with enhanced modulation due to Purcell enhancement. Most demonstrations are near the edge of the 1310 nm telecom band (O-band) [8], [11] or shorter wavelengths [9], [15], [16]. Experiments in the erbium window of the telecom band (C-band) have focused on nanolasers [17]–[19] rather than nanoLEDs. One demonstration at the edge of the erbium window demsonstrated 5 GHz modulation waveguide coupled (with 30% efficiency) from an InGaAs nanopillar encapsulated in a metal cavity [20], unlike the all-dielectric channel cavity in this paper.

4. Advantages and Disadvantages

Having sketched the background, let us summarize the advantages and disadvantages of our waveguided, end-coupled NB LED. The pros and cons are listed as "potential" because the device has not yet been built. Potential advantages are: room temperature operation, emission wavelengths in the new 2 μm band, modulation at speeds in the 1 GHz range as explained below, ultra-small footprint and mode volume, integration on chip including LED arrays, sources that enable the "everything in group IV" PIC, sources that enable entirely monolithic manufacture in CMOS foundries, and sources useful in numerous applications.

Disadvantages include: low or very low emitted-and-waveguided optical power, fairly low wall-plug efficiency, a fairly complex epitaxial layer growth including a possible regrowth of Ge after the LED-segment fabrication, incoherent emission, a spectral emission band that is wider than that of a laser, and the need for wider bandgap connecting waveguides. Advantages will be traded off against disadvantages. When deciding whether the NB LED is appropriate for a particular application, specific advantages will be weighed against specific disadvantages.

5. Diode Structures

It is known from the literature on GeSn electroluminescence that the bulk spontaneous emission lifetime, τ_{sp0}, of an active GeSn LED structure depends upon a group of factors: the alloy composition of the active emitter, the temperature of operation, the degree of strain present in the emitter layer, the doping density of both the P-type and N-type regions, the strength of the electron and hole injection into the active layer, and the confinement of those carriers within the GeSn as determined by the valence band and conduction band offsets between the well and the barriers.

For the present nanoLED, we have room temperature operation, and the alloy composition will be approximately $Ge_{0.94}$ $Sn_{0.06}$ for an unstrained or relaxed emitter that gives peak emission at the 0.61 eV photon energy. Assuming heavily doped P-Ge and N-Ge as the heterodiode claddings, lattice matched to the undoped Ge (on Si) buffer layer, we estimate the τ_{sp0} will be in the range of 10 ns to 100 ns, with 10 ns occurring at high levels of carrier injection. For the case of a compressively strained active emitter, we would utilize a composition of about $Ge_{0.92}Sn_{0.08}$ that is grown pseudomorphic or coherent upon the doped Ge (cladding) barrier, and here the τ_{sp0} would be in the same 10–100 ns range, with a tendency towards the shorter lifetimes.

The valence band and conduction band offsets, and the degree of strain, if any, can be engineered by employing doped barriers of SiGeSn ternary rather than elemental Ge. However, that adds complexity to the LED fabrication. The LED could in principle be a GeSn PIN homojunction diode, but the dual heterostructure Ge/GeSn/Ge PIN diode offers better confinement of injected carriers in GeSn, and is assumed here. Within the NB rib channel, the forward-biased injected diode could be a lateral PIN diode [1], [2], [21] or a diode that is layered in the vertical direction. The horizontal layered approach is taken here as being more practical in the silicon foundry.

Higher radiative efficiency of the LED is attained in multi-quantum well structures or in PINP devices featuring Zener tunnel injection [22]. However, those are not considered here because of their complexity. We shall not discuss the relationship between LED and LD structures, except to

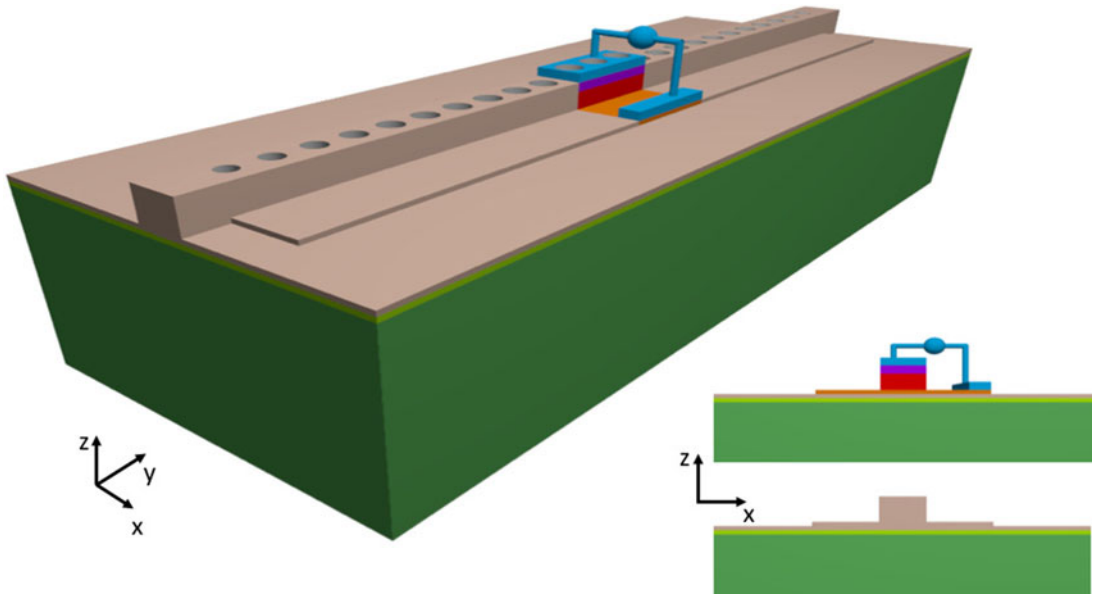

Fig. 1. Perspective view of NB LED and its two output waveguides (Green is SiO_2, light green is Si, light brown is Ge, orange is N-Ge, purple is P-Ge, red is intrinsic GeSn, and blue are the metallic contacts and wires). Inset shows the active region cross-section (top) and the PhC cross section (bottom).

say that the NB resonator is an excellent approach with which to create a GeSn nanocavity LD in the future.

6. Proposed LED Structure

Fig. 1 illustrates the proposed LED structure, comprising a relaxed Ge buffer layer (50 nm) on a thin Si layer (50 nm) upon a "thick" SiO_2 layer that rests on a silicon substrate. The NB in Fig. 1 acts as one continuous, holey, rib-channel waveguide and yet it consists of three joined sections. The central section is the electrically pumped P-Ge/i-GeSn/N-Ge emitter. The first and third sections are undoped Ge rib-channels that end-couple to the three-layer emitter, an emitter that has very smooth, flat, vertical, etched end-facets. Regarding the 50-nm rib platform layer at the bottom of the NB, it is mostly intrinsic Ge, except in the locally doped mid-section where it is N-Ge. This emitter length is typically in the 1.0 to 1.4 μm range as defined by the local doping length. Both the top P-Ge layer and the bottom N-Ge rib layer have the same length.

The heterodiode region in Fig. 1. has two rectangular metal-contact regions that connect to the applied voltage source by wires. The first electrical contact is the metalized exposed top surface of the P-Ge, while the second metal contact area is on one side of the N-Ge rib as shown. The second contact is spaced away from the optical core to minimize damping of the optical mode. The rib extending along the full NB in Fig. 1 provides high Q via optical impedance matching between active and passive sections. As to dimensions, the total NB height is 300 nm, consisting of $(50 + 200 + 50)$ nm in the Ge/GeSn/Ge region where 100 nm of metal (420 nm width) is added locally on top of that core. The NB core width is 420 nm [23]. The rib width is 1600 nm, giving a wing extension of 590 nm on each side of the core. The second metal contact, also 100 nm thick, has a width of 200 nm, leaving a space of 390 nm between metal and core. The top metal is perforated by the PhC air holes. As to the doping density, it is 3×10^{17} cm^{-3} for P-Ge and 4×10^{18} cm^{-3} for N-Ge. The Ge free carrier theory in [24] indicates that the extinction coefficient k in each doped layer is 0.0004 at the emission wavelength of 2 μm.

The 1D PhC consists of a Gaussian taper [25] of cylindrical holes which penetrate through the Ge buffer and the Si layer as well as through the core. The Gaussian taper allows for high coupling of the emitted light from the active region to the Ge ridge waveguides. The lattice constant, a, is

TABLE 1
Refractive Index of NB LED Materials

Material	Index of Refraction n + ik
GeSn	4.25
Ge	4.115
Doped Ge	4.115 + i0.0004
Si	3.44
SiO_2	1.44
Au	0.3003 + i13.4037

350 nm. The symmetric case, 12/12, signifies twelve air holes on each side of cavity center. Our Gaussian taper refers to tapering the diameter of those holes from 0.34*a* in the center to 0.24*a* at each end, forming a "zero point-defect resonator." The active heterolayer region is placed in the center between the two tapers in the strongest mode field. The offset of the active heterolayer region is *a*/2 or zero for the active region length of $L = 1\ \mu$m (1.35 μm) discussed below. The offset of the active region was chosen for the largest cavity quality factor. We also examined an asymmetric NB structure known as 24/12. Taking cavity center as a reference line, there are 24 holes in the left-side NB and 12 holes in the right-side NB. For that device the emitter rectangle is then offset by 5*a*/2 or 2*a* towards the 24 hole side rather for the $L = 1\ \mu$m or 1.35 μm. This is to have the active region overlap with the strongest field. The beginning and end PhC hole sizes remain the same size as in the 12/12 design but with the 24-hole tapering being more gradual over twice as many PhC holes.

The possible fabrication process includes beginning with an area for epitaxy that is larger than the final diode area (later etched to the appropriate size). The three layer horizontal epitaxial layering would consist first of the thin Ge layer that is doped N type. After that the intrinsic GeSn is deposited. Finally there is epitaxy of the top Ge layer that is subsequently locally doped P type. Having formed the PIN structure, it is then etched into its ridge-mesa shape (stopping vertically at N Ge) and this mesa includes parallel vertical ends. This would be following similar processing to that in [26]. The next step is selective area epitaxial regrowth of undoped Ge all around the mesa with a thickness equal to the mesa height. After that, this Ge film is etched into two Ge ridge channel waveguides to complete the waveguide and active region fabrication, apart from the two metal contact strips that are subsequently fabricated by a photolightographic process. Constructing the PhC holes requires electron beam lithography and subsequent etching.

7. Simulation Procedures

The electromagnetic modeling software Lumerical FDTD Solutions [27] was used to simulate the symmetric PhC cavity. A mesh size of 10 nm by 10 nm was used along the width and length of the total NB while the vertical mesh size was 25 nm in the Ge PhC region and 5 nm in the layered active PhC region. The refractive indices of the materials at $\lambda = 2\ \mu$m are given in Table 1 and the background index is 1 for air.

The NB structure was simulated in two phases: (1) with a top contact only, and (2) with top and side contacts. The case (1) had brief computation time, allowing for optimization of the PhC structure, whereas the simulation for (2) was more computationally intense due to the lack of symmetry requiring a significant increase in computation time. It was found that the addition of the side contact reduced the Q without significantly changing the effective mode volume V. It was also

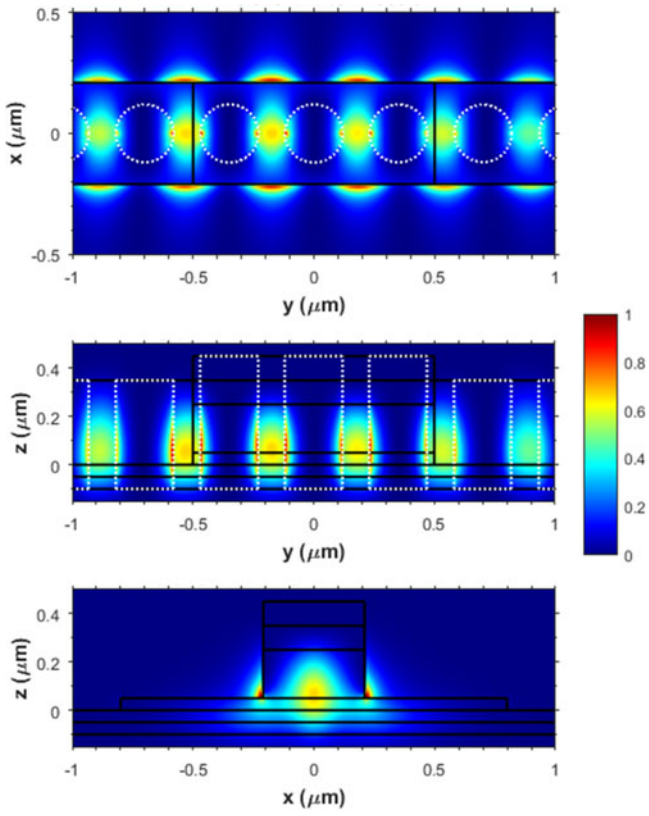

Fig. 2. Normalized profiles of the squared magnitude of the electric field of the cavity. The black outlines the LED materials while the white outlines the PhC holes. From top to bottom: Top-down view of structure with the peak field strength shown (20 nm from GeSn/N-Ge interface), side view of structure with field from center of device, and edge view of the device through active region with field at the peak antinode. $y = 0$ μm in these plots corresponds to the center of the active region.

found that the Q could be increased by lengthening the taper (this was done in 24/12) or by adding additional holes with the same radius as the last in the taper. Case (1) gives an initial indication of behavior. Case (2) is a more realistic scenario. Results for (1) and (2) are given below.

The quality factor, Q, and mode volume, $V = \frac{\int \epsilon E^2}{\max(\epsilon E^2)}$, were extracted from the simulation results using a TE oriented dipole for excitation and built-in analysis tools. Optical electric field cross-sections of the device for case (1) with active region length $L = 1$ μm and an Au top contact are shown in Fig. 2 where the semiconductor materials are outlined with black lines and the air holes are sketched in white. The fields are predominantly TE polarized as is the fundamental waveguide mode.

The height of the Ge and Si layers of the virtual substrate were chosen to minimize the amount of field that "leaks" into the virtual substrate while providing a high quality surface for the epitaxial growths. The height and width of the nanobeam were set such that the Ge waveguide supported the fundamental TE mode at a wavelength of 2 μm. The GeSn height within the active region was chosen such that the largest overlap between the cavity mode and the active region was achieved while minimizing the physical volume which must be electrically pumped. It should be noted that while the 2 μm emission is focused on in this study the peak emission wavelength of this nanoLED is easily tuned or chosen by the selection of the tin content in the GeSn alloy. For example, a particular concentration with the range of 4 to 8% would allow peak emission at room temperature to be in the wavelength range of 1.8 to 2.2 μm. The PhC lattice constant would need to be adjusted such that the cavity resonance matched the emission wavelength.

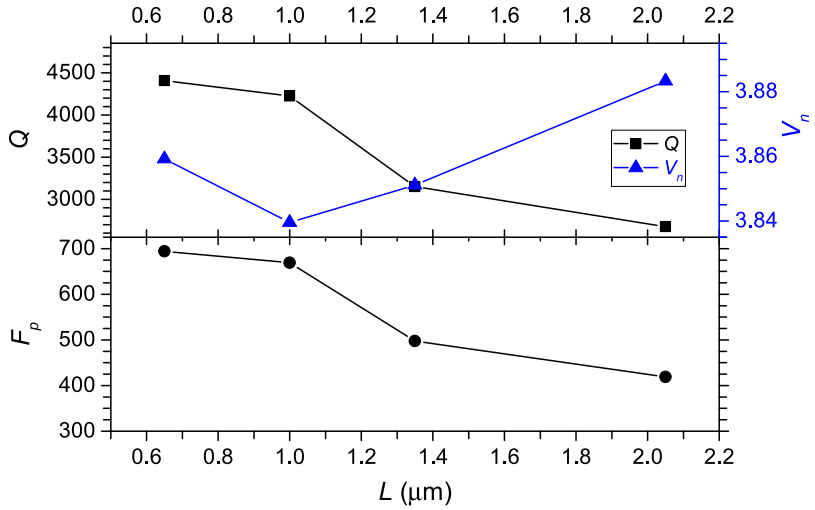

Fig. 3. Cavity quality factor (black squares), effective mode volume in units of effective cubic half-wavelengths (blue triangles), and Purcell factor (black circles) for active region lengths that encompass 1, 2, 3, and 5 antinodes fully. Lines in plots are guides for the eye.

The length of the active region was optimized using the case (1) for the 12/12 structure. Results are shown in Fig. 3 for the Q, V_n, and Purcell enhancement where V_n is the normalized mode volume $V_n = V/(\lambda/2n_{eff})^3$, in terms of effective cubic half-wavelengths, and n_{eff} is the effective index of the NB LED calculated following [28]. Lengths are chosen such that a complete antinode of the cavity is encompassed and while avoiding a material interface intersecting an antinode. The change in V_n over the active region lengths is less than a percent from the average though there is a half percent change between the two shortest active region lengths. The quality factor change is much more significant over the range of active region lengths. The resulting Purcell factors for the two shortest lengths are 694 and 669. Since encompassing two full antinodes doubles the region of the device that can be Purcell enhanced, ignoring the small contributions of the partially encompassed antinodes, with only a 3.6% drop in the Purcell enhancement the $L = 1$ μm is the length which results in the highest modulation rate and a significant emission intensity.

Comparing cases (1) and (2), we found by simulations for the symmetric cavity that top-plus-side contacts reduced the Q by $\sim$ 33% compared to the top-only case, a result caused by added optical mode tailing into lossy metal.

8. Estimated Modulation Speeds

Regarding the electrical equivalent circuit of the NB, we have estimated that the RC time constant of the LED segment is in the picoseconds range. We believe that this RC time is not the limiting factor on modulation speed because the photonic responses computed here are on a longer time scale. We shall now employ the analysis of [3] in order to estimate the maximum speed of direct internal modulation of the NB LED from the cavity quality factor, the cavity mode volume, and the GeSn bulk spontaneous emission lifetime. The 3-dB modulation bandwidth is given by

$$f_{3\mathrm{dB},max} \approx \frac{1}{2\pi\sqrt{\tau_p^2 + \tau_{sp}^2}} \tag{1}$$

where $\tau_p = Q/\omega_o$ is the photon lifetime for emission at a cavity frequency of ω_o and τ_{sp} is the Purcell-enhanced modal spontaneous emission lifetime

$$\tau_{sp} = \frac{\tau_{sp0}}{F_p \beta} \tag{2}$$

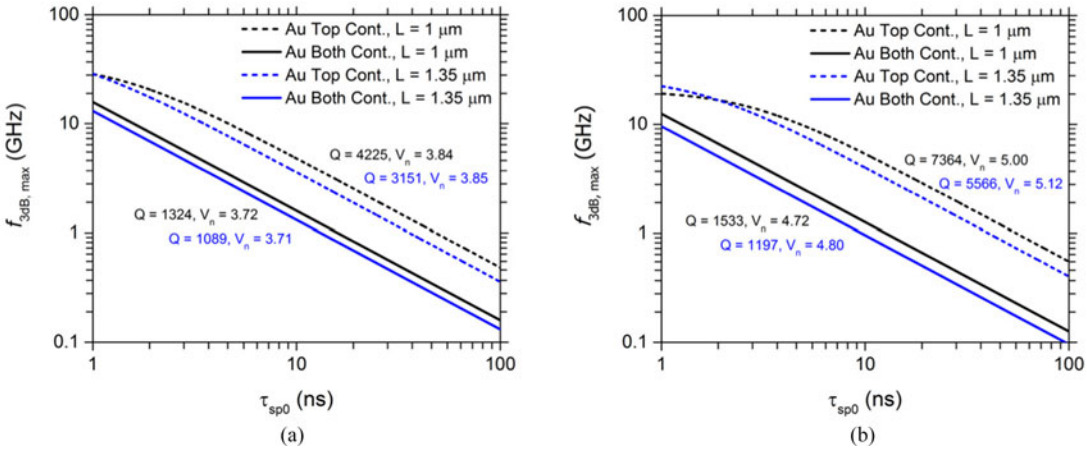

Fig. 4. 3 dB modulation bandwidth as a function of GeSn bulk spontaneous lifetime for two active LED lengths and two contact situations. (a) Shows the results for the symmetric 12/12 PhC design and (b) shows the results for the asymmetric 24/12 PhC design. The corresponding Q and V_n for each cavity are listed.

F_P is the Purcell enhancement given by

$$F_p = \frac{6Q}{\pi V_n} \tag{3}$$

and the parameter β represents fraction of the spontaneous emission that couples to the cavity mode [29]

$$\beta = \frac{1}{1 + \frac{\pi \Delta\lambda V_n}{\lambda}} \tag{4}$$

where $\Delta\lambda$ is the FWHM linewidth of the unenhanced spontaneous emission spectral profile. A typical nanocavity design can be optimized for quality factor while the mode volume varies only slightly for a given design. This leads to an optimization of the cavity Q since the two lifetimes in (1) are inversely proportion to Q. Henceforth in this paper, $\Delta\lambda$ is taken to be 200 nm - being representative of previously reported LED behavior [30]–[32]. This then implies that β is $\sim$0.43 for our device structures. As discussed above, the spontaneous emission lifetime of bulk GeSn is still under study [33] and varies based on growth conditions and electrical excitation conditions. Having examined the GeSn LED literature, we estimate that τ_{sp0} is in the range from 10 to 100 ns at room temperature, with 10 ns representing the best-case scenario that occurs during high $e + h$ injection. The NB Q is highest when using gold contacts, a metal that might be compatible with the back end of a CMOS process. Contacts made of other metals such as Cu or Al or W give Q lower than for Au in our simulations. Those metals are fully CMOS compatible and might be used in a tradeoff of manufacturability versus ultimate speed. The Au results are presented here. In our modulation speed simulations we examined LED lengths of 1.00 and 1.35 μm where $L = 1.00\ \mu$m fully encompasses two antinodes of the cavity and $L = 1.35\ \mu$m encompasses an additional antinode while avoiding an antinode interface. We considered top-only and top-plus-side contacts, and the results are given in Fig. 4.

The increase in the mode volume for the 24/12 PhC design is due to the electric field strength decaying less rapidly outwardly from the active LED length. This can be seen in Fig. 5 where the antinode strength beyond the active region is stronger relative to the peak field than in the 12/12 case. The more gradual Gaussian taper on the 24 hole side of the device leads to a region over $\sim$6 PhC holes where the radius of the PhC holes varies only slightly. The increase in emission coupled to a particular waveguide is at the cost of a slightly reduced peak modulation rate.

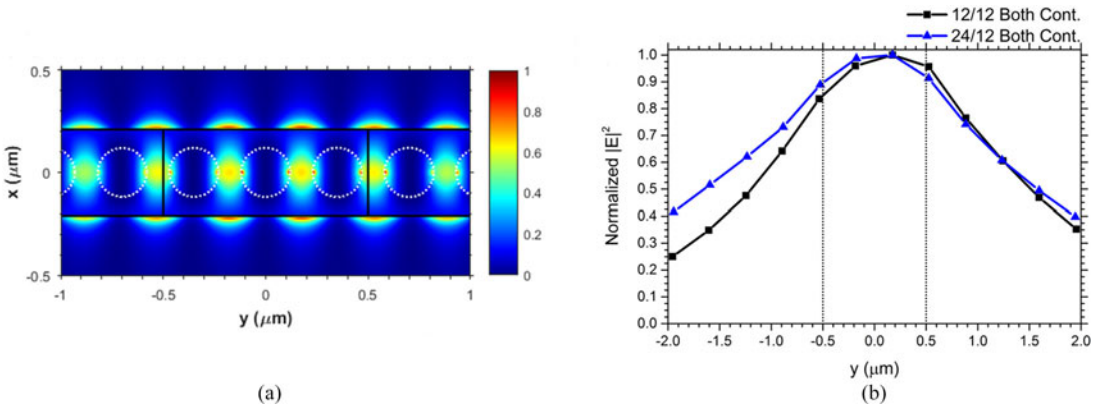

Fig. 5. (a) Normalized top-down profile of the squared magnitude of the electric field of the cavity 20 nm from GeSn/N-Ge interface for the 24/12 asymmetric PhC design. (b) Envelope of the antinode field strength through the center of the device in x and the same z-plane as in (a) of the 12/12 and 24/12 cavities with both contacts. Symbols are peak antinode strengths and lines are a guide to the eye.

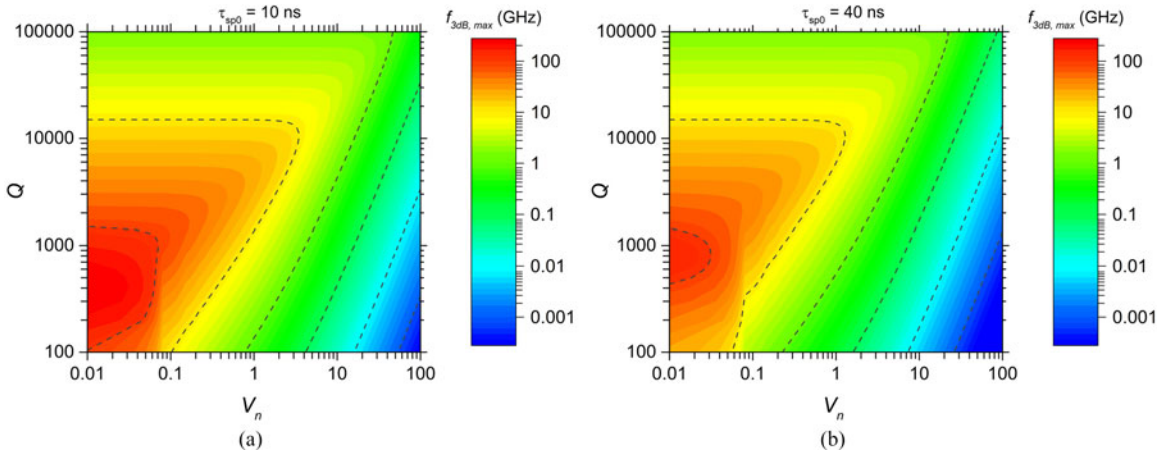

Fig. 6. Modulation bandwidth for bulk GeSn lifetimes of (a) $\tau_{sp0} = 10$ ns and (b) $\tau_{sp0} = 40$ ns for various cavity Q and V_n. Contour lines represent the labelled ticks on the colorbars.

9. Discussion of Speed Results

Examining the results in Fig. 4, two contacts reduces Q vs the one-contact case, but two contacts are in fact essential. As stated in Section VII we shall focus now on $L = 1$ μm as a balance between modulation bandwidth and emission strength. If we now take the range from 10 ns to 40 ns as being realistic for these GeSn NB LEDs then the Fig. 4(a) calculations predict an on-chip direct modulation speed in the range from 1.59 GHz down to 0.40 GHz for the 12/12 symmetric NB device where $\beta = 0.46$ and $V_n = 3.72$. The last group of simulations was performed on the NBs having the asymmetric 24/12 1D-PhC lattice to create the resonant cavity with directional output. Here we find an increase in cavity Q for all test cases but also an increase in the mode volume. The increase in mode volume now limits the max modulation speed to the range from 1.26 GHz down to 0.32 GHz for the directional waveguided emission, as seen in Fig. 4(b), where $\beta = 0.40$ and $V_n = 4.72$. We repeated all of the above simulations for the case in which the spontaneous emission linewidth was 100 nm, and here we found that all of the modulation speeds were ~40% higher than those just cited above. Whether the linewidth of 100 nm or 200 nm is more realistic will be determined by experiments in the future.

If we consider all of the space that surrounds the LED segment, a sphere so-to-speak, and if we examine the total infrared emission, our simulations for the 12/12 case reveal that 30% of the

total is captured by each of the Ge waveguides where that light travels along the channel, while the remaining 40% of the total is lost and radiates into the substrate and the superstrate. In comparison, for the 24/12 case, we find that 49% of the total is confined in the right-side Ge waveguide, while 11% of the total travels within the left-side Ge waveguide. The remaining 40% goes into substrate and superstrate.

Further improvements of the Ge/GeSn PhC NB modulation bandwith require increases in Q or significant reduction of the mode volume. This can seen in Fig. 6 where the modulation rate is explored as a function of Q and V_n at the upper and lower limits of the GeSn lifetime. While reduction of mode volume can be accomplished with a hybrid cavity [14] the introduction of a plasmonic structure adds complexity to both the electrical pumping and fabrication. The most promising candidates for reducing V_n are the slotted NB [34] and a more exotic 1D PhC lattice design within the NB [35] which impact the emitted intensity.

10. Conclusion

A group IV photonics platform for a high modulation-rate PIN heterostructure LED based on bulk GeSn emission has been studied theoretically. Emission of bulk GeSn is coupled into Ge waveguides which also provide the platform for a photonic crystal nanobeam structure. The resonant structure enhances the modulation speed at which the LED can perform compared to traditional bulk LEDs while allowing for integration on a PIC with the 2 μm communication band. It has been shown that operation up to 1.6 GHz is feasible and that directional infrared emission into a single waveguide is achievable with an asymmetric photonic crystal nanobeam at the cost of a slightly lower modulation rate.

References

[1] R. Soref and J. Hendrickson, "Proposed ultralow-energy dual photonic-crystal nanobeam devices for on-chip N $\times$ N switching, logic, and wavelength multiplexing," *Opt. Exp.*, vol. 23, no. 25, pp. 32 582–32 596, 2015.

[2] R. Soref, J. R. Hendrickson, and J. Sweet, "Simulation of germanium nanobeam electro-optical 2 $\times$ 2 switches and 1 $\times$ 1 modulators for the 2 to 5 μm infrared region," *Opt. Exp.*, vol. 24, no. 9, pp. 9369–9382, 2016.

[3] E. K. Lau, A. Lakhani, R. S. Tucker, and M. C. Wu, "Enhanced modulation bandwidth of nanocavity light emitting devices," *Opt. Exp.*, vol. 17, no. 10, pp. 7790–7799, 2009.

[4] T. Suhr, N. Gregersen, K. Yvind, and J. Mørk, "Modulation response of nanoleds and nanolasers exploiting purcell enhanced spontaneous emission," *Opt. Exp.*, vol. 18, no. 11, pp. 11 230–11 241, 2010.

[5] C.-Y. A. Ni and S. L. Chuang, "Theory of high-speed nanolasers and nanoleds," *Opt. Exp.*, vol. 20, no. 15, pp. 16 450–16 470, 2012.

[6] S. A. Fortuna, A. Taghizadeh, E. Yablonovitch, and M. C. Wu, "Toward 100 Ghz direct modulation rate of antenna coupled nanoled," in *Proc. 2016 IEEE Photon. Conf.*, 2016, pp. 216–217.

[7] S. A. Fortuna *et al.*, "Optical antenna enhanced spontaneous emission rate in electrically injected nanoscale III–V led," in *Proc. 2016 Int. Semicond. Laser Conf.* 2016, pp. 1–2.

[8] G. Shambat *et al.*, "Ultrafast direct modulation of a single-mode photonic crystal nanocavity light-emitting diode," *Nature Commun.*, vol. 2, pp. 539-1–539-6, 2011.

[9] C.-H. Liu *et al.*, "Nanocavity integrated van der Waals heterostructure light-emitting tunneling diode," *Nano Lett.*, vol. 17, no. 1, pp. 200–205, 2016.

[10] A. Faraon, E. Waks, D. Englund, I. Fushman, and J. Vučković, "Efficient photonic crystal cavity-waveguide couplers," *Appl. Phys. Lett.*, vol. 90, no. 7, 2007, Art. no. 073102.

[11] G. Shambat *et al.*, "Electrically driven photonic crystal nanocavity devices," *IEEE J. Sel. Topics Quantum Electron.*, vol. 18, no. 6, pp. 1700–1710, Nov./Dec. 2012.

[12] Y. Li *et al.*, "Photonic crystal nanobeam cavity with stagger holes for ultrafast directly modulated nano-light-emitting diodes," *IEEE Photon. J.*, vol. 5, no. 1, Feb. 2013, Art. no. 4 700 306.

[13] W. Da *et al.*, "Horizontally slotted photonic crystal nanobeam cavity with embedded active nanopillars for ultrafast direct modulation," *Chin. Phys. B*, vol. 22, no. 9, 2013, Art. no. 094209.

[14] K. Liu and V. J. Sorger, "Enhanced interaction strength for a square plasmon resonator embedded in a photonic crystal nanobeam cavity," *J. Nanophoton.*, vol. 9, no. 1, 2015, Art. no. 093 790.

[15] M.-J. Yang, C.-C. Lin, Y.-S. Wu, L. Wang, and N. Na, "Optical properties of organic-silicon photonic crystal nanoslot cavity light source," *AIP Adv.*, vol. 7, no. 3, 2017, Art. no. 035309.

[16] S. Nakayama, S. Iwamoto, S. Kako, S. Ishida, and Y. Arakawa, "Demonstration of silicon nanocavity led with enhanced luminescence," in *Proc. Int. Conf. Solid State Devices Mater.*, 2011, pp. 1–8.

[17] K.-Y. Jeong *et al.*, "Electrically driven nanobeam laser," *Nature Commun.*, vol. 4, pp. 2822-1–2822-6, 2013.

[18] W. S. Fegadolli, S.-H. Kim, P. A. Postigo, and A. Scherer, "Hybrid single quantum well InP/Si nanobeam lasers for silicon photonics," *Opt. Lett.*, vol. 38, no. 22, pp. 4656–4658, 2013.
[19] T.-W. Lu, P.-T. Lin, and P.-T. Lee, "Photonic crystal horizontally slotted nanobeam cavity for silicon-based nanolasers," *Opt. Lett.*, vol. 37, no. 4, pp. 569–571, 2012.
[20] V. Dolores-Calzadilla *et al.*, "Waveguide-coupled nanopillar metal-cavity light-emitting diodes on silicon," *Nature Commun.*, vol. 8, pp. 14323-1–14323-8, 2017.
[21] J. Hendrickson, R. Soref, J. Sweet, and W. Buchwald, "Ultrasensitive silicon photonic-crystal nanobeam electro-optical modulator: design and simulation," *Opt. Exp.*, vol. 22, no. 3, pp. 3271–3283, 2014.
[22] R. Koerner *et al.*, "The zener-emitter: A novel superluminescent Ge optical waveguide-amplifier with 4.7 dB gain at 92 mA based on free-carrier modulation by direct Zener tunneling monolithically integrated on Si," in *Proc. 2016 IEEE Int. Electron Devices Meeting*, 2016, pp. 22–25.
[23] M. Kuroki *et al.*, "Germanium photonic crystal nanobeam cavity with $Q > 1{,}300$," in *Proc. 2015 Conf. Lasers and Electro-Opt.*, 2015, Paper SM3G–4.
[24] M. Nedeljkovic, R. Soref, and G. Z. Mashanovich, "Predictions of free-carrier electroabsorption and electrorefraction in germanium," *IEEE Photon. J.*, vol. 7, no. 3, pp. 1–14, Jun. 2015.
[25] Q. Quan, P. B. Deotare, and M. Loncar, "Photonic crystal nanobeam cavity strongly coupled to the feeding waveguide," *Appl. Phys. Lett.*, vol. 96, no. 20, 2010, Art. no. 203102.
[26] C. Chang *et al.*, "Ge0.975Sn0.025 320 $\times$ 256 imager chip for 1.6–1.9 μm infrared vision," *Appl. Opt.*, vol. 55, no. 36, pp. 10 170–10 173, 2016.
[27] "Lumerical Solutions Inc." 2017. [Online]. Available: http://www.lumerical.com/tcad-products/fdtd/
[28] S. G. Johnson, S. Fan, P. R. Villeneuve, J. D. Joannopoulos, and L. Kolodziejski, "Guided modes in photonic crystal slabs," *Phys. Rev. B*, vol. 60, no. 8, pp. 5751–5758, 1999.
[29] E. Yablonovitch, "Light emission in photonic crystal micro-cavities," in *Confined Electrons and Photons*. New York, NY, USA: Springer, 1995, pp. 635–646.
[30] W. Du *et al.*, "Silicon-based $Ge_{0.89}$ $Sn_{0.11}$ photodetector and light emitter towards mid-infrared applications," in *Proc. SPIE*, vol. 10108, 2017, Art. no. 1 010 813–1.
[31] M. Oehme *et al.*, "Room-temperature electroluminescence from GeSn light-emitting pin diodes on Si," *IEEE Photon. Technol. Lett.*, vol. 23, no. 23, pp. 1751–1753, Dec. 2011.
[32] S. Wirths *et al.*, "Lasing in direct-bandgap GeSn alloy grown on Si," *Nature Photon.*, vol. 9, no. 2, pp. 88–92, 2015.
[33] S. Dominici, H. Wen, F. Bertazzi, M. Goano, and E. Bellotti, "Numerical study on the optical and carrier recombination processes in GeSn alloy for E-SWIR and MWIR optoelectronic applications," *Opt. Exp.*, vol. 24, no. 23, pp. 26 363–26 381, 2016.
[34] J. D. Ryckman and S. Weiss, "Low mode volume slotted photonic crystal single nanobeam cavity," *Appl. Phys. Lett.*, vol. 101, no. 7, 2012, Art. no. 071104.
[35] S. Hu and S. M. Weiss, "Design of photonic crystal cavities for extreme light concentration," in *Proc. ACS Photon.*, vol. 3, no. 9, pp. 1647–1653, 2016.